Exploring the Effect of Noise on Geometric Phases using Superconducting Qubits

S. Berger,[1,*] M. Pechal,[1] A. A. Abdumalikov, Jr.,[1] C. Eichler,[1] L. Steffen,[1] A. Fedorov,[1,†] A. Wallraff,[1] and S. Filipp[1]

[1] *Department of Physics, ETH Zurich, CH-8093 Zurich, Switzerland*

(Dated: February 15, 2013)

We make use of a superconducting qubit to study the effects of noise on adiabatic geometric phases. The state of the system, an effective spin one-half particle, is adiabatically guided along a closed path in parameter space and thereby acquires a geometric phase. By introducing artificial fluctuations in the control parameters, we measure the geometric contribution to dephasing for a variety of noise powers and evolution times. Our results clearly show that only fluctuations which distort the path lead to geometric dephasing. In a direct comparison with the dynamic phase, which is path-independent, we observe that the adiabatic geometric phase is less affected by noise-induced dephasing. This observation directly points towards the potential of geometric phases for quantum gates or metrological applications.

PACS numbers: 03.65.Vf, 03.67.Lx, 42.50.Pq, 85.25.Cp

arXiv:1302.3305v1 [quant-ph] 14 Feb 2013

Noise is ubiquitous in physical systems—be it thermal noise in electrical circuits [1], electronic shot noise in mesoscopic conductors [2], vacuum noise of radiation fields [3], or low-frequency (1/f-) noise in solid state systems [4, 5]. It prevents quantum coherence to persist on long time scales [6, 7] and hinders the development of a large-scale quantum computer. Significant effort has thus been put into concepts and methods to control and maintain fragile quantum superposition states [8]. The geometric phase is a promising building block for noise-resilient quantum operations [9] and its properties in open quantum systems have been actively investigated in theory [10–17] as well as in recent experiments [18, 19].

We examine the physics of a spin one-half particle in an effective magnetic field $\mathbf{B}$, described by the Hamiltonian

$$H = \hbar\boldsymbol{\sigma}\cdot\mathbf{B}/2, \tag{1}$$

where $\boldsymbol{\sigma} = (X, Y, Z)$ are the Pauli matrices, and $\mathbf{B} = (B_x, B_y, B_z)$ is given in units of angular frequency. If the magnetic field is adiabatically and cyclically varied in time, the ground $|0\rangle$ and excited state $|1\rangle$ of the spin-half particle acquire a geometric phase $\gamma_0 = \pm A/2$, where A is the solid angle (with respect to the origin $\mathbf{B} = 0$) enclosed by the path traced out by $\mathbf{B}(t)$ [20].

Here, we consider an effective magnetic field evolving along a circular path with radius $B_\rho = \sqrt{B_x^2 + B_y^2}$ at constant B_z and with precession period τ (Fig. 1). This path encloses a solid angle $A = 2\pi(1 - \cos\vartheta)$, with the polar angle $\vartheta = \arctan(B_\rho/B_z)$. The noise is described by fluctuations in the effective magnetic field which are directed either in azimuthal direction φ [angular noise, Fig. 1(b)] or in radial direction ρ [amplitude noise, Fig. 1(c)]. This choice allows us to maximize (respectively minimize) geometric dephasing, as discussed below.

Both types of noise are modelled by an Ornstein-Uhlenbeck process, i.e. a stationary, gaussian and markovian process with a lorentzian spectrum of bandwidth Γ_i and noise power P_i $(i = \rho, \varphi)$. Perturbative treatment of the noise and adiabatic evolution of the spin one-half particle require that the precession frequency and the noise bandwidth are small compared to the amplitude $B = |\mathbf{B}|$ of the effective magnetic field, i.e. $1/\tau, \Gamma_i \ll B$. With these assumptions, the deviation $\delta\gamma$ of the geometric phase to first order in the noise variations $\delta\varphi$ and $\delta\rho$ is [11]

$$\delta\gamma = -\frac{\pi}{\tau}\int_0^\tau \sin\vartheta\,\delta\vartheta\,\mathrm{d}t. \tag{2}$$

As the ensemble average of $\delta\gamma$ vanishes, the mean of the geometric phase is identical to γ_0. Expressing the effective magnetic field in cylindrical coordinates, $\mathbf{B} = (B_\rho\cos\varphi, B_\rho\sin\varphi, B_z)$, the variations in the polar angle can be written as $\delta\vartheta = (\cos\vartheta/B)\delta\rho$, and the geometric phase is found to have a gaussian distribution with variance

$$\sigma_\gamma^2 = 2P_\rho\left(\frac{\pi\cos\vartheta\sin\vartheta}{B\tau}\right)^2\frac{\Gamma_\rho\tau - 1 + e^{-\Gamma_\rho\tau}}{\Gamma_\rho^2}. \tag{3}$$

To first order, only variations $\delta\rho$ in radial direction contribute to σ_γ^2. This can be understood intuitively: Radial noise modifies the enclosed solid angle and hence also the geometric phase. In contrast, noise in the azimuthal angle φ causes variations in the precession frequency of the magnetic field, but no change in the enclosed solid angle—the geometric phase is not affected. Note that the evolution of the magnetic field can be non-cyclic because angular fluctuations at the start of the path are not equal to those at the end. As a result, the geometric phase depends on the solid angle encompassed by the path closed by the great circle connecting the projections of $\mathbf{B}(t = 0)$ and $\mathbf{B}(t = \tau)$ on the unit sphere [21] [Fig. 1(b)]. This deviation from the unperturbed solid angle adds a small contribution to the dephasing [11].

Similarly, the deviation $\int_0^\tau \delta B/\hbar\,\mathrm{d}t = \int_0^\tau \sin\vartheta_0\delta\rho/\hbar\,\mathrm{d}t$ of the dynamic phase δ can be used to compute its mean

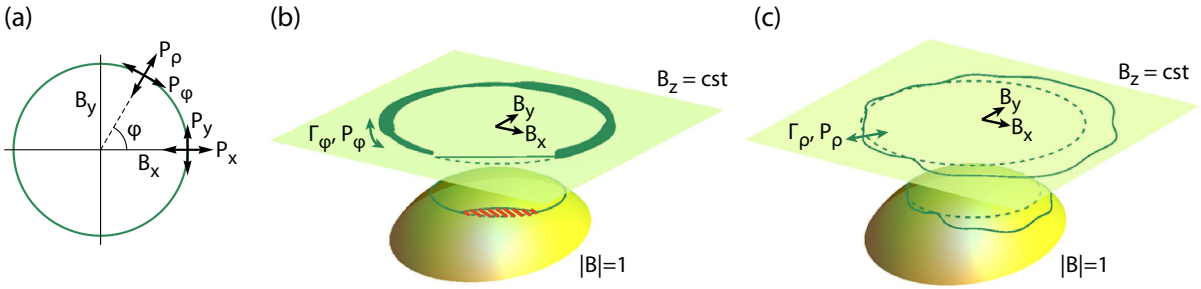

FIG. 1. (a) The path of the effective magnetic field (green line) describes a circle in the B_x-B_y-plane at constant B_z. Noise in x and y directions with noise powers P_x and P_y can be decomposed into noise in ρ and φ directions with noise powers P_ρ and P_φ. (b,c) The path of the magnetic field without noise (dashed green lines lying in the plane with constant B_z) is drawn alongside the same path exposed to two kinds of noise (solid green lines): angular noise in (b), where the velocity of precession is proportional to line thickness, and radial noise in (c). The projection of the paths on the unit sphere $|\mathbf{B}| = 1$ is also shown. In (b), the difference in solid angle due to non-cyclic evolution is highlighted in red.

and its variance

$$\sigma_\delta^2 = 2P_\rho(\sin\vartheta)^2\frac{\Gamma_\rho\tau - 1 + e^{-\Gamma_\rho\tau}}{\Gamma_\rho^2}. \qquad (4)$$

Again, only radial variations contribute to σ_δ^2 and cause the dynamic phase to have a gaussian distribution around the noiseless dynamic phase δ_0. Noise along φ does not change the magnitude of the field and hence does not cause fluctuations in the dynamic phase.

The geometric phase has been observed in a variety of superconducting systems [22–25]. In the experiment presented here, the spin one-half particle is formed by the two lowest energy levels of a superconducting artificial atom of the transmon type [26] embedded in a transmission line resonator—an architecture known as circuit quantum electrodynamics [27, 28]. The qubit is manipulated using microwave fields applied via a capacitively coupled charge bias line. Using spectroscopic measurements, we have determined the maximum Josephson energy $E_{J,\max}/h = 11.4\,\mathrm{GHz}$, the charging energy $E_C/h = 0.26\,\mathrm{GHz}$ and the coupling strength $g/2\pi = 360\,\mathrm{MHz}$ of the qubit to the resonator. Its transition frequency between ground and excited state $\omega_{01} = E_{01}/\hbar$ is adjusted using a superconducting coil mounted beneath the sample. The experiments are performed at $\omega_{01} = 4.68\,\mathrm{GHz}$, with an energy relaxation time $T_1 = 2.65\,\mu\mathrm{s}$, a phase coherence time $T_2 = 1.35\,\mu\mathrm{s}$ and a spin-echo phase coherence time $T_2^{\mathrm{echo}} = 2.15\,\mu\mathrm{s}$. The sample is operated in a dilution refrigerator at a base temperature of 20 mK. In the dispersive regime, when E_{01} is far detuned from the resonator mode, the Hamiltonian of the driven system is [22]

$$H_{\mathrm{eff}} = \hbar\left(X\Omega\cos\varphi + Y\Omega\sin\varphi + Z\Delta\right)/2 \qquad (5)$$

in a reference frame which rotates at the drive frequency ω_d. This Hamiltonian is identical to the one in equation (1) with an effective magnetic field $\mathbf{B} = (\Omega\cos\varphi, \Omega\sin\varphi, \Delta)$. It is determined by amplitude Ω, angle φ and detuning $\Delta = \omega_{01} - \omega_d$ of the drive.

A Ramsey-type interferometric sequence containing a spin-echo pulse to cancel the dynamic phase [18, 29] is employed to measure the geometric phase acquired by the spin one-half particle [Fig. 3(a)]. A series of resonant pulses (of frequency ω_{01}) implement the spin-echo sequence, while off-resonant pulses (of frequency $\omega_d = \omega_{01} - \Delta$) guide its state adiabatically along the paths sketched in Fig. 1(b,c).

All presented geometric phases are measured at a detuning $\Delta = -50\,\mathrm{MHz}$. The acquired geometric phase is varied from 0 rad to 6.9 rad by increasing the solid angle A via the drive amplitude Ω. The strength of the noise is quantified by the normalized noise amplitude $s_\rho = \sqrt{P_\rho}/B_\rho$ for radial noise and by $s_\varphi = \sqrt{P_\varphi}$ for angular noise. These definitions ensure that fluctuations in radial or azimuthal directions have identical amplitudes if $s_\rho = s_\varphi$.

The phases with noise are obtained by repeating the experiment with different noise patterns. Identical noise patterns are used before and after the spin echo pulse to ensure cancellation of the dynamical phase. The pulse sequences, consisting of two intermediate-frequency quadratures x and y, are created by adding numerically generated noise with engineered spectrum, bandwidth and amplitude, to the pulses describing the noiseless evolution of the magnetic field. An arbitrary waveform generator is employed to synthesize these quadratures, which are upconverted to a microwave-frequency signal using an in-phase/quadrature mixer. After the manipulation sequence, the state of the qubit is determined in a dispersive readout [30] through the resonator and reconstructed using state tomography [31]. To overcome noise in the detection, each individual noise realization is measured 10^6 times.

Histograms of the measured geometric phase for four solid angles are shown in Fig. 2(a-d). For radial noise, the geometric phases of the individual noise realizations have—as discussed above—a gaussian distribution with a mean equal to the geometric phase γ_0 without noise. For

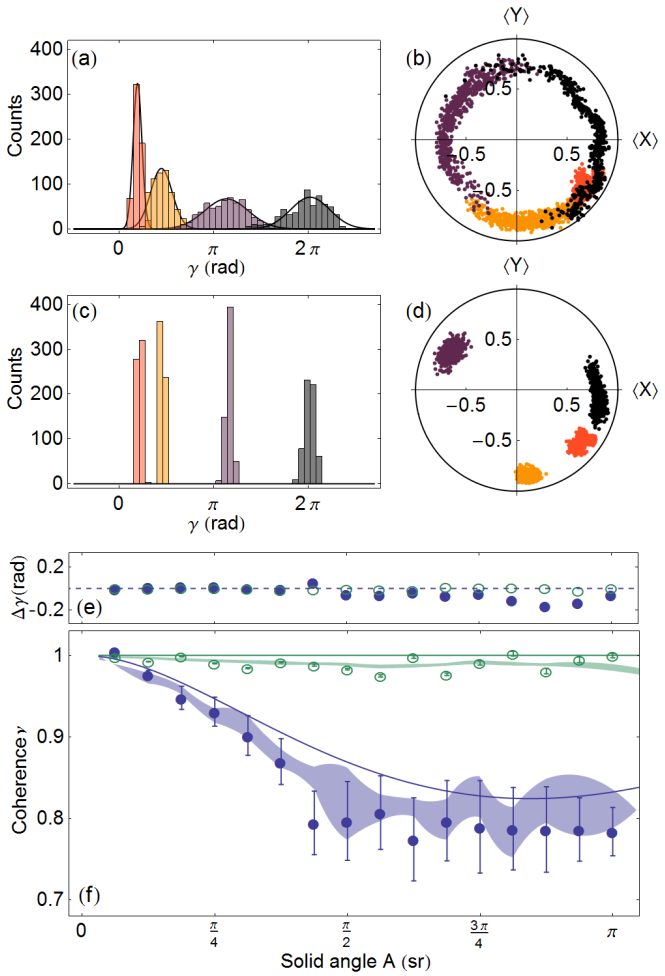

FIG. 2. (a) Histograms of geometric phases and (b) measured expectation values $\langle X\rangle$, $\langle Y\rangle$ of 600 realizations of radial noise for each solid angle $A = \pi/16, 3\pi/16, 8\pi/16$ and $15\pi/16$ (indicated in red, orange, purple and black). Fits of a gaussian to the measured histograms are also shown in (a). The circle in (b) indicates unit coherence. (c,d) Measurements analogous to panels (a,b) for angular noise. (e,f) Coherence ν and phase difference $\Delta\gamma$ as a function of solid angle A for radial noise (filled blue circles) and angular noise (open green circles). The experimental data points are shown alongside the theory curve (solid lines) and the results from numerical simulations (the shaded area indicates the standard deviation about the mean). Data in panels (a-f) is recorded at fixed noise bandwidths $\Gamma_i = 10\,\mathrm{MHz}$, normalized noise amplitudes $s_i = 1/15$ and evolution time $\tau = 100\,\mathrm{ns}$.

angular noise, we observe that the widths of the phase distributions are, as expected, almost zero. The expectation values of the Bloch-vector components $\langle X\rangle$ and $\langle Y\rangle$ for individual noise realizations are distributed on the equatorial plane of the Bloch sphere (Fig. 2b,d), reflecting the spread of the measured phases. They lie on a circle with radius $\nu_0 \approx 0.80 < 1$, which is a result of the intrinsic noise present in the system.

Distributions akin to those shown in Fig. 2(b,d) are used to compute the coherence $\nu = \sqrt{\langle X\rangle^2 + \langle Y\rangle^2} = e^{-(4\sigma_\gamma)^2/2}$ versus solid angle [Fig. 2(f)]. In this plot and all subsequent plots, the coherences are normalized to a measurement without added noise whereby the intrinsic noise is eliminated. We observe that for radial noise the coherence decreases and then stabilizes as a function of solid angle, while it is approximately unity for angular noise. This is an immediate consequence of the nature of the geometric phase: radial noise modifies the solid angle A causing dephasing and a decrease in coherence. In contrast, angular noise hardly affects A. For both kinds of noise, the difference $\Delta\gamma = \gamma - \gamma_0 \lesssim 0.2$ rad in the mean geometric phase with and without noise is very small [Fig. 2(e)]. The measured coherences agree well with the theory from equation (3) and numerical results obtained by solving the unitary dynamics of the Hamiltonian in equation (5). The measured geometric phase γ_0 itself agrees well with the prediction for a transmon-type qubit [25], with an discrepancy of 0.20 rad across all solid angles for the data in Fig. 2(e,f).

To illustrate the effects of noise quantitatively, the geometric and dynamic phases are measured for varying noise amplitudes s. For the geometric phase, we observe that the coherence follows the expected dependence $e^{-(4as)^2/2}$ for radial noise [Fig. 3(c,e)] and that angular noise has a lesser effect on the coherence than radial noise. For both types of noise, the geometric phase with and without noise agrees for normalized noise amplitudes $\lesssim 0.5$.

The coherence of the dynamic phase was recorded using a spin-echo sequence containing a single off-resonant pulse (Fig. 3b), and therefore its variance was scaled by a factor to allow for direct comparison with the geometric phase. From Fig. 3(e), it is evident that the coherence of the dynamic phase starts decreasing at weaker noise amplitudes than the geometric phase, demonstrating the superior noise resilience of the geometric phase. It is also observed that the mean dynamic phase δ starts deviating from δ_0 already at $s \approx 0.2$. The measured coherences for both dynamic and geometric phase are in very good agreement with the theoretical predictions based on equations (3) and (4) for radial noise. For angular noise, fits to $e^{-(4as)^2/2}$ agree with the observed behaviour of the coherences. Indeed, while according to equations (3) and (4) the coherences are expected to be insensitive to angular noise to first order, non-adiabatic and higher-order effects still affect the coherences.

Finally, we directly compare the coherence of dynamic and geometric phases in the presence of radial noise. The geometric phase γ is recorded at a solid angle $A = 0.37\pi$, where the effect of noise on γ is strongest. For long evolution times τ, the geometric phase is more resilient against radial noise than the dynamic phase because its variance σ_γ^2 decreases with evolution time [18], whereas the variance of the dynamic phase σ_δ^2 grows linearly in evolution

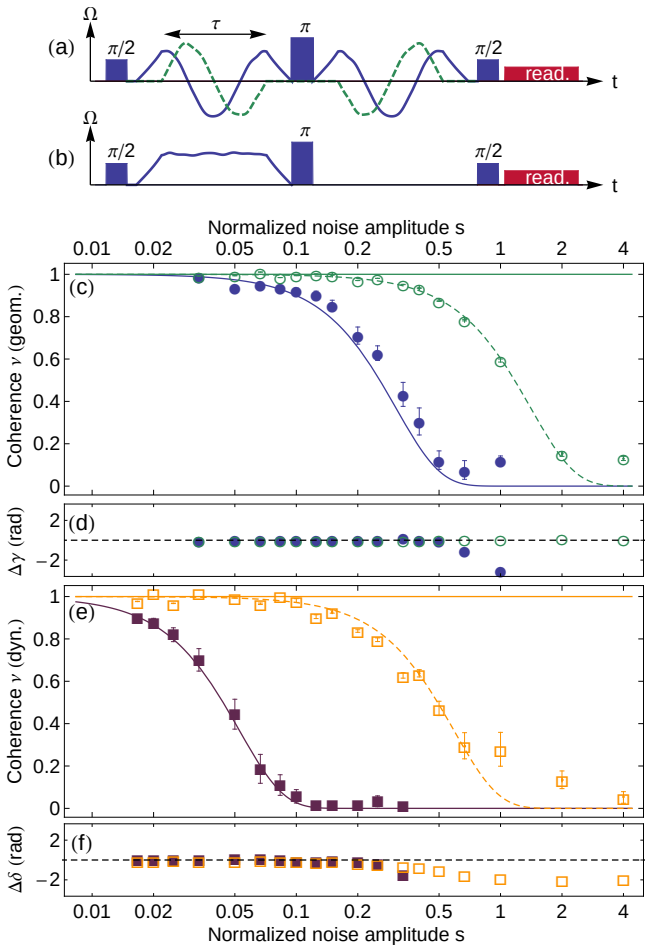

FIG. 3. (a,b) Sketches of the pulse schemes used to measure (a) geometric and (b) dynamic phases with radial noise. Pulses applied along the x and y quadratures are shown in blue and green, respectively. The readout pulse (red, see text) concludes the sequence after $t \approx 400$ ns. (c,d) Experimentally measured coherence ν of the geometric phase and phase difference $\Delta\gamma = \gamma - \gamma_0$ as a function of normalized noise amplitude s for amplitude noise (filled blue circles) and angular noise (open green circles), plotted on a logarithmic scale. For every value of s, 300 noise realizations were measured with noise bandwidth $\Gamma = 10\,\mathrm{MHz}$ at solid angle $A = 7\pi/16$ and evolution time $\tau = 100\,\mathrm{ns}$. The continuous line is theory (Eq. 3). The dashed line is a fit to the function $\exp(-(4as)^2/2)$ with fitting parameter $a = 0.25 \pm 0.01$. (e,f) Results analogous to panels (c,d) for the dynamic phase, with $\Delta\delta = \delta - \delta_0$ and fitting parameter $a = 0.60 \pm 0.03$.

time (cf. equations (3) and (4), as well as Fig. 4). Both phases perform equally well when $\sigma_\gamma^2 = \sigma_\delta^2$, i.e.

$$\tau = \pi \cos(\vartheta)/B, \tag{6}$$

and the dynamic phase only outperforms the geometric phase for even shorter evolution times ($\tau < 13$ ns according to equation (6) and $\tau < 20$ ns according to the experimental data in Fig. 4). Note that the variance of

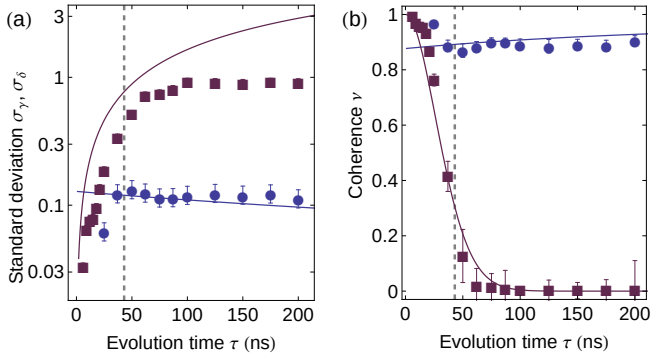

FIG. 4. (a) Standard deviation σ_γ of the geometric phase (blue circles) and σ_δ of the dynamic phase (purple squares) as a function of evolution time τ, based on 300 noise realizations with $\Gamma = 10\,\mathrm{MHz}$ and $s_\rho = 1/15$. The theory curves are shown as solid lines. The dashed grey line approximately separates the non-adiabatic from the adiabatic regime. (b) Coherence ν versus evolution time τ. The labelling is analogous to panel (a).

the dynamic phase is independent of the value of the dynamic phase, this is why it was recorded using the same drive amplitudes as for the geometric phase gates. The data in Fig. 4 agrees well with theory. The standard deviation σ_δ of the dynamic phase starts differing from theory at evolution times $\tau \gtrsim 100\,\mathrm{ns}$, when the recorded phases are spread across 2π and their variance saturates.

In conclusion, we have made use of a superconducting qubit to demonstrate that the geometric phase is less affected by noise along the qubit path than by noise perpendicular to it. Given a system with known noise properties, this can potentially be exploited to realize noise-resilient geometric gates for quantum information processing. Both kinds of noise leave the mean of the geometric phase unchanged. Shifts of the mean geometric phase are theoretically expected [12], but are beyond current experimental precision. We have also shown that the geometric phase outperforms the dynamic phase in terms of noise resilience when evolving adiabatically (evolution times $\gtrsim 1/B$). Our results beautifully exemplify a fundamental property of the geometric phase, namely its dependence on the enclosed area in the parameter space, and serve as a stepping-stone for further investigations of the geometric phase as a resource for quantum computation or as a metrology device [32, 33].

* sberger@phys.ethz.ch
† Current address: School of Mathematics & Physics, The University of Queensland, Brisbane QLD 4072, Australia

[1] F. N. H. Robinson, *Noise and fluctuations in electronic devices and circuits*, edited by Oxford (Clarendon Press, 1974).

[2] Y. M. Blanter and M. Büttiker, Physics Reports **336**, 1 (2000).
[3] R. J. Glauber, Phys. Rev. **130**, 2529 (1963).
[4] P. Dutta and P. M. Horn, Rev. Mod. Phys. **53**, 497 (1981).
[5] J. Bylander, S. Gustavsson, F. Yan, F. Yoshihara, K. Harrabi, G. Fitch, D. G. Cory, Y. Nakamura, J.-S. Tsai, and W. D. Oliver, Nature Physics **7**, 565 (2011).
[6] M. Schlosshauer, *Decoherence and the Quantum-to-Classical Transition* (Springer, Heidelberg Berlin, 2007).
[7] E. Joos, H. D. Zeh, C. Kiefer, D. J. W. Giulini, J. Kupsch, and I.-O. Stamatescu, *Decoherence and the appearance of a classical world in quantum theory* (Springer, Heidelberg & Berlin, 2003).
[8] T. D. Ladd, F. Jelezko, R. Laflamme, Y. Nakamura, C. Monroe, and J. L. O'Brien, Nature **464**, 45 (2010).
[9] E. Sjöqvist, Physics **1**, 35 (2008).
[10] A. Blais and A. M. S. Tremblay, Phys. Rev. A **67**, 012308 (2003).
[11] G. De Chiara and G. M. Palma, Phys. Rev. Lett. **91**, 090404 (2003).
[12] R. S. Whitney, Y. Makhlin, A. Shnirman, and Y. Gefen, Phys. Rev. Lett. **94**, 070407 (2005).
[13] R. S. Whitney and Y. Gefen, Phys. Rev. Lett. **90**, 190402 (2003).
[14] A. Carollo, I. Fuentes-Guridi, M. F. Santos, and V. Vedral, Phys. Rev. Lett. **90**, 160402 (2003).
[15] P. Solinas, M. Möttönen, J. Salmilehto, and J. P. Pekola, Phys. Rev. B **82**, 134517 (2010).
[16] P. I. Villar and F. C. Lombardo, Phys. Rev. A **83**, 052121 (2011).
[17] P. Solinas, M. Sassetti, P. Truini, and N. Zanghì, New J. Phys. **14**, 093006 (2012).
[18] S. Filipp, J. Klepp, Y. Hasegawa, C. Plonka-Spehr, U. Schmidt, P. Geltenbort, and H. Rauch, Phys. Rev. Lett. **102**, 030404 (2009).
[19] F. Cucchietti, J.-F. Zhang, F. Lombardo, P. Villar, and R. Laflamme, Phys. Rev. Lett. **105**, 240406 (2010).
[20] M. V. Berry, Proc. R. Soc. Lond. **A392**, 45 (1984).
[21] J. Samuel and R. Bhandari, Phys. Rev. Lett. **60**, 2339 (1988).
[22] P. J. Leek, J. M. Fink, A. Blais, R. Bianchetti, M. Göppl, J. M. Gambetta, D. I. Schuster, L. Frunzio, R. J. Schoelkopf, and A. Wallraff, Science **318**, 1889 (2007),.
[23] M. Möttönen, J. J. Vartiainen, and J. P. Pekola, Phys. Rev. Lett. **100**, 177201 (2008).
[24] M. Neeley, M. Ansmann, R. C. Bialczak, M. Hofheinz, E. Lucero, A. D. O'Connell, D. Sank, H. Wang, J. Wenner, A. N. Cleland, M. R. Geller, and J. M. Martinis, Science **325**, 722 (2009).
[25] S. Berger, M. Pechal, S. Pugnetti, A. A. Abdumalikov Jr., L. Steffen, A. Fedorov, A. Wallraff, and S. Filipp, Phys. Rev. B **85**, 220502(R) (2012).
[26] J. Koch, T. M. Yu, J. Gambetta, A. A. Houck, D. I. Schuster, J. Majer, A. Blais, M. H. Devoret, S. M. Girvin, and R. J. Schoelkopf, Phys. Rev. A **76**, 042319 (2007).
[27] A. Blais, R.-S. Huang, A. Wallraff, S. M. Girvin, and R. J. Schoelkopf, Physical Review A **69**, 062320 (2004).
[28] A. Wallraff, D. I. Schuster, A. Blais, L. Frunzio, R.-S. Huang, J. Majer, S. Kumar, S. M. Girvin, and R. J. Schoelkopf, Nature (London) **431**, 162 (2004).
[29] J. A. Jones, V. Vedral, A. Ekert, and G. Castagnoli, Nature **403**, 869 (2000).
[30] R. Bianchetti, S. Filipp, M. Baur, J. M. Fink, M. Göppl, P. J. Leek, L. Steffen, A. Blais, and A. Wallraff, Physical Review A **80**, 043840 (2009).
[31] M. G. A. Paris and J. Řeháček, eds., *Quantum State Estimation*, Lect. Notes Phys, Vol. 649 (Springer, Berlin, Heidelberg, 2004).
[32] A. E. Martín-Martínez, A. Dragan, R. B. Mann, and I. Fuentes, arXiv:1112.3530v1 (2011).
[33] X. Rong, P. Huang, X. Kong, X. Xu, F. Shi, Y. Wang, and J. Du, Europhys. Lett. **95**, 6 (2011).